Applied Catalysis B: Environmental 193 (2016) 170–179

Contents lists available at ScienceDirect

Applied Catalysis B: Environmental

journal homepage: www.elsevier.com/locate/apcatb

Influence of the support on PtSn electrocatalysts behavior: Ethanol electro-oxidation performance and *in-situ* ATR-FTIRS studies

Elen Leal da Silva[a,*], Andrés Cuña[a,b], Maria Rita Ortega Vega[a], Claudio Radtke[c], Giovanna Machado[d], Nestor Tancredi[b], Célia de Fraga Malfatti[a]

[a] LAPEC/PPGE3M, Universidade Federal do Rio Grande do Sul, Av. Bento Gonçalves, 9500, Setor 4, Prédio 75, Sala 232, 91501-970 Porto Alegre, RS, Brazil
[b] Cátedra de Fisicoquímica, DETEMA, Facultad de Química, Universidad de la República—Avenida General Flores 2124, CC 1157, Montevideo 11800, Uruguay
[c] Instituto de Química, Universidade Federal do Rio Grande do Sul, Av. Bento Gonçalves, 9500, 91501-970 Porto Alegre, RS, Brazil
[d] Centro de Tecnologias Estratégicas do Nordeste—CETENE, Av. Professor Luis Freire, 01, 50740540 Recife, PE, Brazil

ARTICLE INFO

Article history:
Received 1 December 2015
Received in revised form 5 April 2016
Accepted 11 April 2016
Available online 14 April 2016

Keywords:
PtSn
Activated biocarbons
Ethanol electro-oxidation mechanism
In-situ ATR-FTRIS

ABSTRACT

Different activated biocarbons (aBCs) were prepared from *Eucalyptus grandis* wood and activated Vulcan carbons (aVCs) were prepared from commercial Vulcan XC72 carbon. These carbon materials were used as a support in a PtSn/C electrocatalysts for ethanol electro-oxidation (EEO). Structural, morphological and chemical composition differences of the electrocatalysts were correlated to their electrocatalytic performance, and by *in-situ* Fourier Transform Infrared Spectroscopy in the Attenuated Total Reflectance mode (*in-situ* ATR-FTIRS), with the ethanol electro-oxidation mechanism (EEOM) pathways and product distributions at different potentials using sulfuric acid as a base electrolyte.

The nature of the carbon support and it activation method affected the morphological and structural characteristics of the PtSn based electrocatalysts. The electrocatalytic performance of the electrocatalysts supported on the aBCs was better than that of the supported on the activated Vulcan carbons. The PtSn electrocatalysts using CO_2 activated biocarbon support had a higher electrochemically active surface area (EASA), lower onset potential and greater current density for the EEO. It was determined that the EEO on all studied PtSn electrocatalysts in sulfuric acid media occurs mainly through the acetic acid and acetaldehyde production.

1. Introduction

The use of different supports can yield very different electrocatalytic performances in direct ethanol fuel cells (DEFCs) [1,2]. However, there is a variety of materials with potential as catalyst support for DEFCs anode: nanofibers [3], nanotubes [4], graphene [5] and activated carbons [6]. Their main requirements for DEFCs anode catalyst support are high electrical conductivity, high surface area and chemical stability [7].

On the other hand, biomass and waste materials are renewable resources available in large quantities and at low cost. A few years ago, the evaluation of biomass residues led to use it as a starting material to produce activated biocarbons (aBCs) for different applications (adsorbents, supercapacitors, *etc.*) [8–12]. In recent years, we reported the use of aBCs obtained from *Eucalyptus grandis* wood as a Pt and PtSn supports for ethanol electro-oxidation, and we demonstrated a better electrocatalytic performance for the aBCs support electrocatalysts compared to the Vulcan carbon electrocatalysts support (traditional support) [6].

Activated carbons can be obtained by different synthetic routes in which process variables can be set in order to reach desired final properties, such as porous texture and/or surface chemistry. Anyway, different final properties of the carbon catalysts support can affect the dispersion and particle size of the metallic catalysts, its poisoning susceptibility, electrolyte accessibility to the catalytic active site, electrocatalytic active surface area, catalyst stability and electron transfer [13–15]. These different characteristics of the electrocatalysts can determine differences in their catalytic activity including the ethanol electro-oxidation mechanism (EEOM) on its surface [16].

In-situ Fourier Transform Infrared Spectroscopy (*in-situ* FTIRS) is a dynamic technique that can allow the study of the physicochemical changes in a solid/liquid interface as a function of an external electric field [17,18]. *In situ*-FTIRS has been successfully used to obtain qualitative and quantitative data on electrochemi-

* Corresponding author at: Av. Bento Gonçalves, 9500, DEMET, Prédio 75, Sala 232, CEP 91501-970 Porto Alegre, RS, Brazil.
E-mail address: elenlealdasilva@gmail.com (E. Leal da Silva).

http://dx.doi.org/10.1016/j.apcatb.2016.04.021
0926-3373/

Table 1
Carbons and activated carbons used as catalyst supports.

Carbon support	Precursor	Activation method
p-V	Carbon Vulcan XC72	Physical activation in CO_2
p-BC	*Eucaliptus g* wood	atmosphere, at 800 °C for 2 h
c-V	Carbon Vulcan XC72	Chemical activation with $ZnCl_2$ for
c-BC	*Eucaliptus g* wood	1 h at 900 °C in N_2 atmosphere

cal surface processes such as the electro-oxidation of small organic molecules [18]. One variation of this technique is the *in-situ* FTIRS in the Attenuated Total Reflectance mode (*in-situ* ATR-FTIRS), which appropriate technique to perform *in-situ* FTIRS measurements for non-reflective surface like the carbon supported catalysts [16]. In recent years, some authors have reported the use of *in-situ* ATR-FTIRS, following different methodologies, to study the EEOM pathways and determine the product distributions at different potentials as a function of the electrocatalysts structure and composition [16,19–23]. Many of the EEOM *in-situ* ATR-FTIRS studies have been reported for the ethanol electro-oxidation using perchloric acid as a base electrolyte. However, the anion of the base electrolyte can have an effect on the mechanism of electro-oxidation of small organic molecules such as ethanol [23] or methanol [18]. Until now, EEOM studies for electrocatalysts with aBCs as support material and using sulfuric acid as base electrolyte has not been reported.

In this work, different aBCs were prepared from *E. grandis* wood by chemical and physical activation. Also, activated Vulcan carbons (aVCs) were prepared from commercial carbon Vulcan XC72, using the same method and conditions that were employed for aBCs. These carbon materials were characterized by textural and elemental analysis, and they were used as a carbon support in a PtSn/C electrocatalysts for ethanol electro-oxidation. The electrocatalysts morphology and composition were determined by X-ray diffraction (XRD), transmission electron microscopy (TEM), Rutherford backscattering spectrometry (RBS) and termogravimetric analysis (TGA). Structural, morphological and chemical composition differences of the electrocatalysts were correlated to their electrocatalytic performance, and by *in-situ* ATR-FTIR, with the EEOM pathways and product distributions at different potentials in a 1.0 mol L^{-1} ethanol + 0.5 mol L^{-1} H_2SO_4 solution.

2. Experimental

2.1. Electrocatalysts support preparation

Table 1 describes the aVCs and the aBCs used as catalysts supports and the synthetic routes for their obtaining. Before de biocarbon activation, the *E. grandis* wood was ground, sifted and then dried at 105 °C for 24 h. The used activation methods were based in the previous described procedures [12,24].

2.2. Electrocatalysts preparation

Electrocatalysts synthesis was already explained in a former work [25]. Impregnation/reduction method was employed, using ethylene glycol as reduction agent and $H_2PtCl_6{\cdot}6H_2O$, $SnCl_2{\cdot}2H_2O$ salts as catalyst precursors. Adequate amounts of support and salts were mixed together to obtain an electrocatalyst with a Pt:Sn atomic ratio of 4:1 with a metal charge of 40 wt%.

2.3. Support characterization

2.3.1. Textural analysis

The supports porous texture was determined by N_2 adsorption/desorption isotherm at 77 K, with a Beckman Coulter SA 3100 equipment. For mesoporous samples, Brunauer–Emmet–Teller (BET) equation was used, and the total pore volume (V_T) at relative pressure of 0.99 and specific surface area (S_{BET}) were determined. Mean pore size (*dp*) was determined by [26]:

$$dp(nm) = \frac{4000 V_T \left(\frac{cm^3}{g}\right)}{S_{BET}\left(\frac{m^2}{g}\right)} \quad (1)$$

For microporous samples, microporous surface area (S_{mic}), micropore volume (W_o) and the average micropore width (L_0) were determined by the Dubinin-Radushkevich equation [27].

2.3.2. Elemental analysis

Elemental composition (nitrogen, hydrogen, carbon and sulfur) was determined with a Thermo Scientific Flash 2000 equipment. Ash content was determined according to ASTM D2866/2011 [28]. The oxygen content was determined by difference.

2.4. Electrocatalysts characterization

2.4.1. Rutherford backscattering spectrometry (RBS)

The RBS analyses were performed using a He+ beam at 2 MeV produced by TANDEM accelerator of 3 MV. In all the cases, the incidence beam was perpendicular to the sample surface and the detection angle was 165° related to beam direction.

2.4.2. Termogravimetric analysis (TGA)

In order to determine the catalysts mass percentage in the electrocatalysts, TGA was performed on the catalysts supported systems using a Shimadzu TG-50 in dynamic air atmosphere, in the temperature range from 298 to 1123 K using 5 K min^{-1} heating rate, with sample masses between 8.0 and 10.0 mg in alumina crucible. The constant mass at the end of the thermogravimetric curve was related to the amount of catalyst present in the sample.

2.4.3. Structural and morphological analysis

X-ray diffraction analysis was made with a Philips, X'Pert MPD equipment, operating with Cu-Kα radiation, generated with 40 kV and 40 mA. X-ray diffractogram allows establishing the crystal structure assumed by the catalyst inside the support. Morphological information for the catalysts was obtained with an FEI Tecnai Spirit Biotwin G2 TEM, operating at 100 kV.

2.5. Electrochemical and spectroelectrochemical characterization

2.5.1. Electrocatalytic performance

The electrochemically active surface area (EASA) of the electrocatalyst was determined by cyclic voltammetry in 0.5 mol L^{-1} H_2SO_4 solution at 10 mV s^{-1} in the potential range from −0.2 to 0.8 V *vs.* the saturated calomel electrode (SCE) [29]. A three-electrode cell, with platinum as the counter electrode and Saturated Calomel Electrode (SCE) as the reference electrode, was used in the experiments. As a working electrode, a graphite disk with 0.29 cm^2 in area, covered with a mixture of electrocatalyst powder Nafion® was used. The graphite disk was placed in Teflon support to carry out electrochemical analyses. The preparation procedure for the working electrode consisted in a 5 mg of dispersed electrocatalyst particles (supported on carbon) in 2 mL ethanol (Merck) and 25 μL of Nafion (5% by weight, Aldrich). This solution was placed in an ultrasonic bath to homogenize the material and aliquots of the mixture were added to the graphite disk.

EASA was determined by the Eq. (2),

$$EASA = \frac{charge\,(\mu C\,cm^{-2})}{[210\,(\mu C\,cm^{-2}Pt)\,\times\,(electrode\,loading\,(g\,Pt\;cm^{-2})]} \quad (2)$$

Table 2
Textural and elemental analysis of the activated carbons and activated biocarbons.

Sample	Textural Analysis				Elemental Analysis (mass percentage, dry basis)					
	V_T or W_o (cm^3/g)	S_{BET} (m^2/g)	S_{mic} (m^2/g)	d_p or L_o (nm)	C	H	N	S	Ash	O[a]
Vulcan XC72	0.44	216	–	8.2	96.4	0.6	0.0	0.6	2.1	0.3
p-V	0.39	230	–	6.9	96.4	0.5	0.0	0.4	2.4	0.3
c-V	0.47	221	–	8.6	93.2	0.9	0.1	0.6	3.1	2.1
E. grandis	–	–	–	–	49.5	6.5	0.0	0.0	0.4	43.6
p-BC	0.47	787	–	2.4	82.2	1.7	0.0	0.0	6.1	10.0
c-BC	0.51	–	752	1.3	89.8	0.9	0.0	0.0	0.6	8.7

[a] Determined by difference.

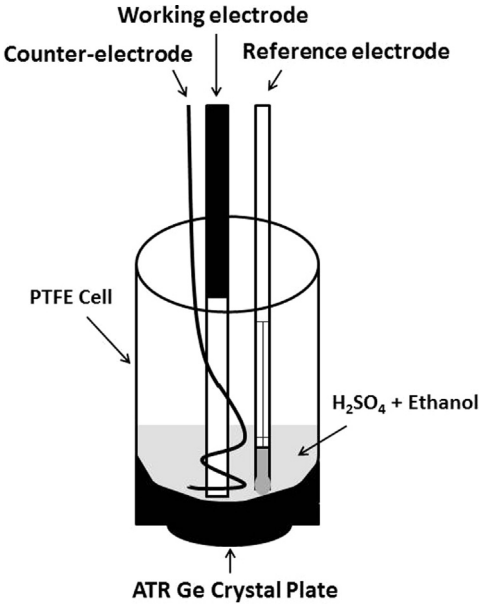

Fig. 1. Experimental arrangement for linear sweep voltammetry and for *in-situ* ATR-FTIRS measurements.

where charge ($\mu C\,cm^{-2}$) is the charge per unit area of electrode associated to the hydrogen adsorbed/desorbed peaks in the voltammogram, and the electrode loading ($g\,Pt\,cm^{-2}$) is the Pt mass per unit area of electrode. The charge of 210 $\mu C\,cm^{-2}$ corresponds to the hydrogen monolayer adsorbed on Pt [30]. In this work, the EASA was calculated from the oxidation branch of the cyclic voltammetry.

Linear sweep voltammetry was done in order to determine the electrochemical behavior of the catalyst in 1.0 mol L^{-1} ethanol + 0.5 mol L^{-1} H_2SO_4 solution. Measurements were carried out using a three-electrode cell as described in Fig. 1, with platinum wire as counter-electrode and saturated Ag/AgCl as reference electrode. As working electrode a graphite disk was used with a geometric area of 0.29 cm^2, which was coated with a mixture of electrocatalyst powder in Nafion®. The experiments were done with scan rate of 10 mV s^{-1}, in a potential range from −0.2 to 1.0 V. In order to eliminate the oxygen present in the medium, nitrogen was bubbling inside the solution since 10 min before. Chronoamperometry experiments were performed using 0.5 mol L^{-1} H_2SO_4 +1.0 mol L^{-1} ethanol at 0.40 V over 60 min.

All the electrochemical measurements were performed at 25 °C, on a potentiostat/galvanostat AUTOLAB PGSTAT 302N.

2.5.2. Spectroelectrochemical experiments

The spectroelectrochemical *in-situ* ATR-FTIRS measurements were carried out at 25 °C using a Bruker Vertex 70 V spectrometer equipped with a Mercury-Cadmium-Telluride (MCT) liquid N_2 cooled detector and ATR Ge crystal plate. ATR Ge window was used because is suitable for this experiments from the viewpoint of chemical resistance to the electrolyte solution used (0.5 mol L^{-1} H_2SO_4 +1.0 mol L^{-1} ethanol) and allow adequate detection of the most important FTIR bands for the all EEO expected products.

The experimental setup used in this work was similar to that used by De Souza et al. [16], using the same working electrodes and electrolytes that were used in the linear sweep voltammetry experiments. The spectra were collected as the ratio R:R_0, where R represents a spectrum at a given potential, and R_0 is the spectrum collected at −0.15 V *vs.* Ag/AgCl electrode. Positive and negative directional bands represent gains and losses of species at the sampling potential, respectively. The spectra were computed from 32 interferograms averaged from 4000 cm^{-1} to 800 cm^{-1} with the spectral resolution set to 4 cm^{-1}. Initially, a reference spectrum (Ro) was measured at −0.15 V, and then sample spectra were collected after applying successive potential steps from 0.0 to 1.0 V *vs.* Ag/AgCl electrode.

3. Results and discussion

3.1. Support characterization

The results of the textural and elemental analysis of the aVCs, aBCs and their precursors are shown in Table 2. The S_{BET} value for sample c-BC is not included in Table 2 because, for microporous carbon materials (pore diameter less than 2 nm) as the c-BC sample, is not advisable to apply the BET equation being more desirable determining the surface area for this type of sample by the Dubinin-Radushkevich method [27,31]. That is why for this sample was placed the value of the microporous surface area S_{mic} instead the S_{BET}.

It is observed a significant difference in specific surface area and pore size between the aBCs and aVCs supports. The aBCs had a higher surface area and a smaller pore size than aVCs. The c-BC sample developed a microporous texture (L_0 = 1.3 nm), while the p-BC had a texture located at the bottom limit of mesoporosity with a 2.4 nm pore diameter. For p-V and c-V supports, the mean pore diameter was 6.9 and 8.6 nm respectively.

In general, aVCs had higher carbon and ash content, but lower oxygen content. The ash content of p-BC sample is a bit higher than expected for this type of biocarbon. However it is expected an increase in the percentage of ash content compared to the wood due to a "concentration effect" of the ashes present in the wood after the wood pyrolysis. The ashes found in an activated carbon prepared from wood by physical activation with CO_2 as p-BC sample, can only come from the inorganic components of the own wood (mainly K, Mg and Ca for *E. grandis* wood) which can form ash such as $K_2Ca(CO_3)_2$, MgO and $CaCO_3$ [32,33]. Anyway, there is no scientific evidence that this type of ash can have a catalytic effect on the ethanol electro-oxidation (EEO).

It was observed that the sulfur content was not negligible for the aVCs. The different aVCs had similar compositions to their precursor (Vulcan XC72). The sulfur content in the aBCs was zero due

Table 3
Atomic ratio and catalysts mass percentage of the eletrocatalysts.

Sample	Nominal Composition (atomic, 100%)	Experimental Composition (atomic, 100%)[a]	PtSn (mass%)	Pt (mass ratio%)
PtSn/p-V	Pt:Sn 79:21	Pt:Sn 80:20	40	35
PtSn/c-V	Pt:Sn 79:21	Pt:Sn 72:28	40	32
PtSn/p-BC	Pt:Sn 79:21	Pt:Sn 76:24	40	34
PtSn/c-BC	Pt:Sn 79:21	Pt:Sn 81:19	44	38

[a] Determined by RBS analysis.

Table 4
Lattice parameters and crystallite size of the catalysts obtained by X-ray diffraction.

Sample	Lattice parameter (Å)	Crystallite size (nm)
PtSn/p-V	3.94	3.00
PtSn/c-V	3.94	2.33
PtSn/c-BC	3.93	4.16
PtSn/p-BC	3.95	3.15

to the biomass precursor, being an important advantage from an environmental point of view. The higher carbon content and the lower oxygen and hydrogen content of the c-BC with respect to the p-BC was expected due to the higher maximum activation temperature (900 °C) of the c-BC sample compared to the p-BC (800 °C), which determined a higher oxygenated and hydrogenated compounds devolatilization of the precursor material [12].

3.2. Electrocatalysts characterization

Rutherford Backscattering Spectroscopy analyses were carried out aiming to determine the percentage composition of metals in the electrocatalysts, and by TGA to determine the catalysts mass in the electrocatalysts. The results are summarized in Table 3.

It was found that the composition determined by RBS analysis (Table 3) was fairly similar to the nominal composition shifts. The amount of catalysts supported on the different activated carbons are according to the metallic charge (40 wt%) used in the synthesis. These results suggest that the impregnation/reduction method using ethylene glycol as a reducing agent is a suitable method for obtaining nanoparticles of PtSn.

X-ray diffractograms for the supported metallic catalysts are shown in Fig. 2.

It can be seen the diffraction peaks located at 39, 46, 68 and 81 which correspond to the planes (1 1 1) (2 0 0) (2 2 0) (3 1 1) of platinum, representing a typical platinum cubic face centered crystal structure [29,34,35]. Compared with the reference Pt/C, in the studied electroctalysts these peaks are shifted at lower 2θ angle values. In the inset of Fig. 2 this behavior can be clearly seen for the peak located at 39°. Lattice parameter and crystallite size computations are explained in former work [6]. The values obtained for the samples studied in this work appear in Table 4. The studied electrocatalysts had higher average lattice parameter value *a* and thus dilatation of the crystallite lattice as compared with pure platinum values (3.91 Å) [6]. These results are in agreement with the literature, where the PtSn peak shift was assigned to the alloying between platinum and tin, indicating a PtSn alloy formation and not only a Pt or Sn separate deposition [36,37].

The electrocatalyst PtSn/c-V also presents small peaks around 2θ = 34 and 52, which are consistent with the SnO_2 phase [38,39]. For the other electrocatalysts these peaks are not observed, but the presence of amorphous tin oxides cannot be discarded.

Comparing the XRD diffractograms with RBS results, it can be seen that there is no direct relation between the Sn content (determined by RBS) in the different electrocatalysts with the shift in the XRD peaks. A sample with higher content of Sn (determined by RBS) will not necessarily show a higher shift in the XRD peaks. This fact arises from the distinct information obtained by XRD and RBS. XRD probes only crystalline phases while RBS, the areal concentration of the probed element irrespectively of the phase of the material.

In summary, these results show that the ethylene glycol reduction method produces nanoparticles in the desired size range for applications in DEFCs [29].

PtSn support surface dispersion and particle size were estimated from examination of TEM images shown in Fig. 3, using ImageJ software. The particles are with average sizes of 3.4 nm for p-V and c-V, 2.5 nm for p-BC and 3.5 nm for c-BC. These results agree with those reported for PtSn alloy supported on different types of carbon materials [20,40], and it is consistent with the mean crystallite sizes calculated from XRD data.

In TEM images, for all samples it can be seen a large catalyst particle agglomeration on the support surface. This agglomeration is more strong on the activated biocarbons supports, were PtSn particles agglomeration are present throughout the whole support, when compared to the ones on the Vulcan-based carbons, where the catalyst deposition was more agglomerated on some regions of the support. This fact can be explained based on differences in surface area, pore size microstructure and surface chemistry of the supports.

aBCs have a larger surface area than the activated Vulcan carbons, as they have microporous surface area with narrow pores, while activated Vulcan carbon surface area is mainly associated with much larger mesopores. Therefore, in the case of aBCs a great part of its surface area will not be accessible for the reactant during the synthesis of the electrocatalyst, especially for large molecules as $PtCl_6^{2-}$ (anion precursor in the PtSn) [41] and the tin salt. It may determine a lower surface area available for creating nucleation sites, which allow localization throughout the whole aBC support. The predominant mesoporous texture of the Vulcan-based activated carbons, with higher values of pore size compared to the biocarbons, worked out as pathways for the catalyst precursor salts to reach the specific sites for the metal reduction.

In addition, the highest content of oxygenated functional groups of the aBCs, determined by elemental analysis (Table 2), may have a negative effect on the degree of catalyst dispersion on the support surface [2,42]. Román-Martínez et al. [43] reported the reduction of Pt from the $PtCl_6^{2-}$ precursor on the carbon basal planes. In this sense, there is an hindrance stablished by the oxygenated surface functional group, for the metallic precursor to reach those carbon basal planes, due to the repulsion between the catalyst precursor molecules and the oxygen atoms on the biocarbon surface [43,44]. This behavior it could also apply for the PtSn catalyst, since Pt is the main component of the alloy.

Heterogeneity in microstructure is also a crucial factor regarding catalyst dispersion and agglomeration. According to Stoeckli [45], microporous carbons obtained from vegetable sources tend to be more heterogeneous than carbon blacks. Since the biocarbons studied in this work are prone to be more microporous, it is expected heterogeneity in its structure. Likewise, considering that the Vulcan-based carbons come from the burning of hydrocarbons [41] and its carbon content is very high compared to the biocarbons, they can be regarded as carbon blacks, having an ordered distribution pattern of carbon layer planes [42]. These authors also point out that carbon blacks are formed by small nuclei that determine each

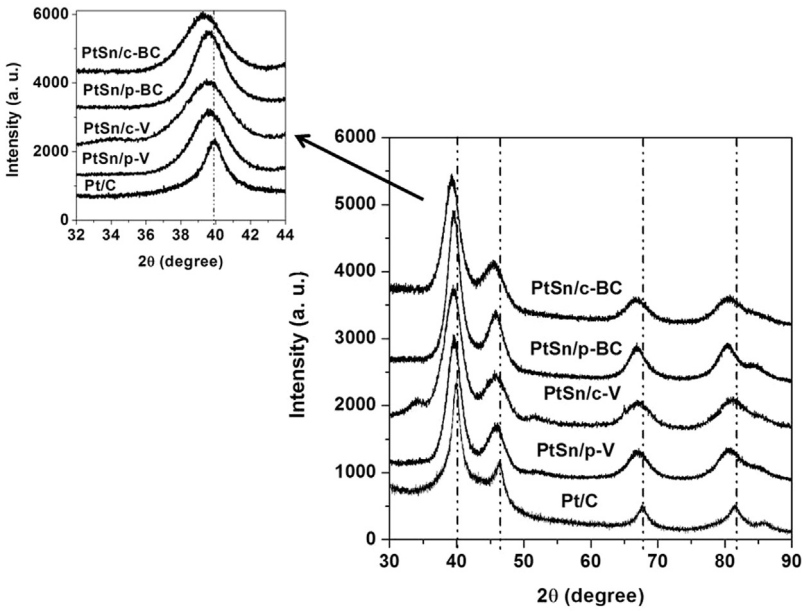

Fig. 2. X-ray diffraction patterns of PtSn/C electrocatalysts and Pt/C reference.

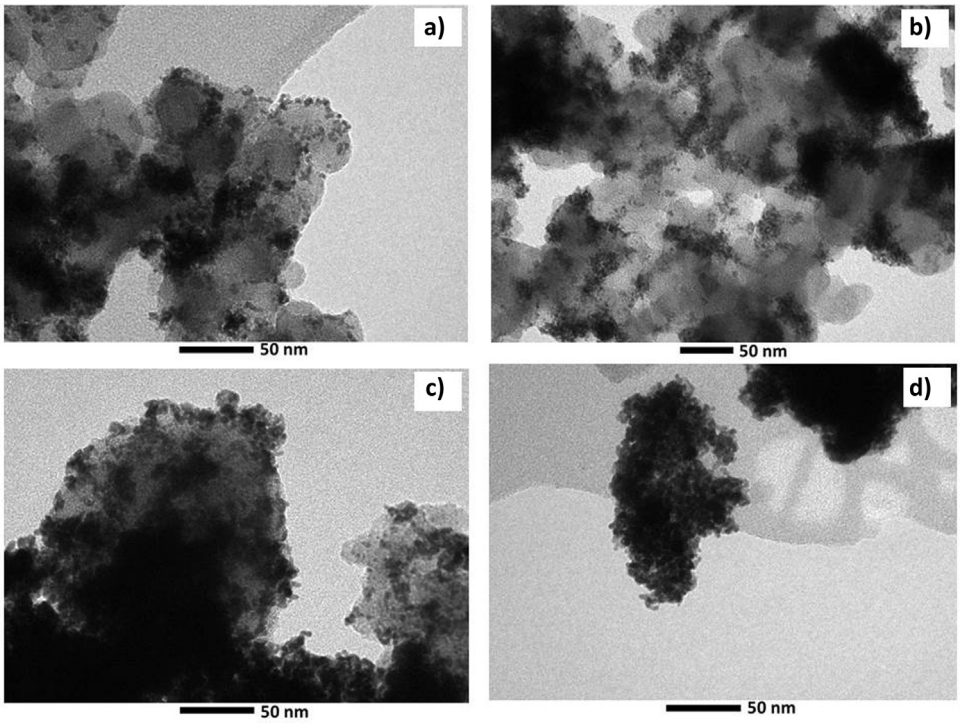

Fig. 3. Images obtained from TEM (a) PtSn/p-V, (b) PtSn/c-V, (c) PtSn/p-BC and (d) PtSn/c-BC.

plane orientation [42]. With thermal treatments like those applied in the activation methods, the ordering achieved is higher [42,44]. Since the PtSn deposition and agglomeration in the Vulcan-based carbons were more located as suggested by the TEM images (Fig. 3), it is possible to state that the nucleation of the catalyst nanoparticles, in a preference site on the support surface, is influenced by the structural pattern of carbon planes offered by the support. For the biocarbons, as it was aforementioned, the metallic catalyst is settled throughout the support surface, influenced by the disorganized structure of the support.

3.3. Electrocatalytic performance

The voltammetries obtained in the absence of ethanol, shown in Fig. 4, display the typical profile of the hydrogen absorption/desorption on carbon supported PtSn. Even though the voltammetries were carried out using the SCE reference electrode, in order to facilitate the reading and comparison along the article, the potential in the obtained voltammograms are plotted *vs.* the Ag/AgCl reference electrode. All electrocatalysts showed a peak between −0.155 V and 0.145 V *vs* Ag/AgCl electrode that is in agree-

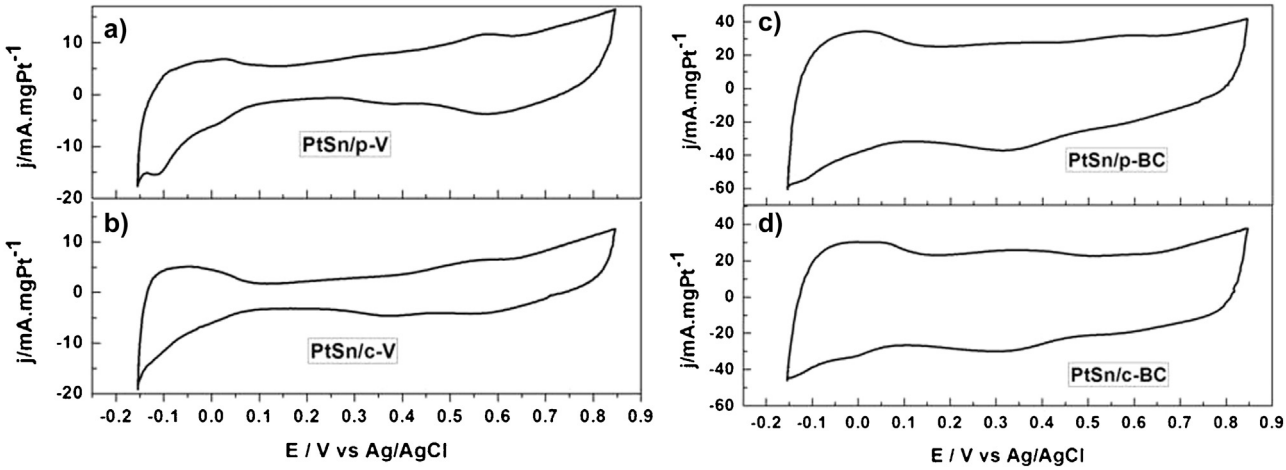

Fig. 4. Cyclic voltammograms of the electrocatalysts in a 0.5 mol L^{-1} H_2SO_4 solution at a scan rate of 10 mV s^{-1} and T = 25 °C.

Table 5
Electrocatalysts active surface area and maximum current density (i_{max}) and onset potential (E_{onset}) determined for ethanol electro-oxidation in 0.5 mol L^{-1} H_2SO_4 +1.0 mol L^{-1} ethanol.

Sample	EASA (m^2 g Pt^{-1})	i_{max} (mA mg Pt^{-1})	E_{onset} (V) *vs.* Ag/AgCl
PtSn/p-V	30.25	79.5	0.35
PtSn/c-V	22.91	72.0	0.32
PtSn/p-BC	200.40	106.6	0.10
PtSn/c-BC	100.23	91.5	0.15

ment with previous reports [29]. It can also be seen that there is a difference in the shape of the curves obtained for the BCs supported catalysts (Fig. 4c and d) compared to the Vulcan supported catalysts samples (Fig. 4a and b). The curves obtained for the BCs supported catalyst show a higher capacitive contribution. This behavior is due to the higher specific surface area of the BCs (752 and 787 m^2 g^{-1}) compared to the Vulcan carbons (221 and 230 m^2 g^{-1}). As is well known, the higher the specific surface area of the carbon material the higher the capacitive contribution due to the electrochemical double layer formation at the carbon surface-electrolyte interface [46,47]. Consequently, in the calculation of EASA for the BCs supported catalysts, the capacitive contribution was subtracted. From the area under these peaks and with the Eq. (2), the EASA was determined. The corresponding values, expressed per unit mass of Pt, are shown in Table 5. aBCs supported catalysts have higher EASA values compared with those supported on aVCs, and in both cases, meanwhile the catalysts supported on physically activated carbons have slightly higher EASA than those supported on the chemically activated ones.

Fig. 5 shows the results of the linear sweep voltammograms at 10 mV s^{-1} obtained for EEO on electrocatalysts at 1 mol L^{-1} of ethanol concentration. In order to better visualization of the onset potentials, an inset (with a magnification between −0.1 and 0.5 V *vs* Ag/AgCl) was added in Fig. 5. From these curves, onset potential (E_{onset}) and the maximum current density value (i_{max}) appear in Table 5. The i_{max} was determined at 1.0 V for all samples except for the PtSn/c-V which determined at 0.89 V because it is in this potential that the sample has developed its maximum current density.

The onset potentials values determined for PtSn/p-BC and PtSn/c-BC samples are 0.1 and 0.15 V respectively. These onset potential values are not contradictory with the fact that both materials have the same catalytic activity between 0.18 and 0.4 V. The onset potential is related to the thermodynamics of the ethanol electro-oxidation reaction while the current density values observed in linear sweep voltammetry will also be influenced by the kinetics of the process [48]. The onset potential for the ethanol electro-oxidation reaction (EEOR) on the biocarbon supported PtSn is lower than the values determined for the aVCs supported catalysts. Therefore, the thermodynamics of EEOR is more favored on the biocarbon supports, preferentially on the one obtained by physical activation. For the Vulcan-based carbons, the onset potential values are very close. The measured current density in the potential range of 0.0–0.74 V *vs.* Ag/AgCl electrode is highest for the aBCs supported PtSn catalysts, consistent with the greater EASA obtained for these samples (see Table 5). As it is seen in Fig. 5, the current density is the same (56 mA mg Pt^{-1}) for all the samples in approximately 0.74 V. Furthermore, the current density increase rate, from 0.4 V to about 0.74 V, is higher for the catalysts supported on the aVCs than for the aBCs. It makes that the current density of all samples is approximately equal to 0.74 V. The lower current density increase rate for the PtSn/aBCs is probably related to the smaller support pore size. In consequence, there is a decrease in the rate of EEOR due to a lower reactant and product diffusion to and from the catalyst surface, and to the steric hindrance in the adsorption-desorption process.

At about 0.46 V it is possible to observe a shoulder in the PtSn/p-BC curve. This shoulder is related to the current generated by a rapid ethanol electro-oxidation around this potential. This fact will be further discussed and related to the results of the spectroelectrochemical analysis.

In general terms, the better catalytic performance (lower E_{onset} and higher current density) observed for the aBCs supported electrocatalysts can be attributed to their higher EASA and to the change in the electronic structure of the catalyst induced by the support. This last fact can conduct to a lower binding energy between the Pt in the PtSn catalyst and the carbon atoms of the intermediates formed during the EEO, which determines a lower catalyst poisoning [2].

Fig. 6 shows the chronoamperometric curves for EEO on PtSn/C electrocatalysts obtained by polarization at 0.4 V for 60 min. These results are in agreement with the results obtained from the linear sweep voltamograms (Fig. 5). BCs supported catalysts showed similar electrocatalytic activity and they developed higher current density and stability than the Vulcan supported catalysts. For the Vulcan supported samples, a decrease in the oxidation current density with time is observed above 5 min. This fact is specially marked for the PtSn/c-V sample, thus indicating a possible poisoning of nanocatalyst but, for a precise conclusion on this issue, additional experiments must be made in future works.

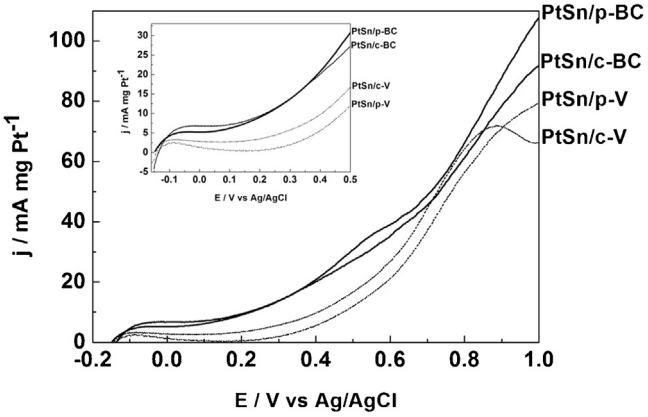

Fig. 5. Linear sweep voltammograms of different electrocatalysts.

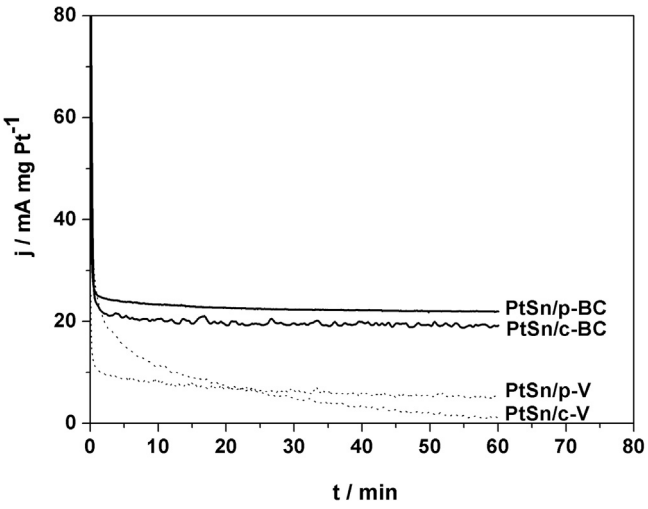

Fig. 6. Chronoamperometry curves at 0.40 V for the different electrocatalysts in 0.5 mol L^{-1} H_2SO_4 +1.0 mol L^{-1} ethanol, time = 60 min and T = 25 °C.

3.4. Spectroelectrochemical results

Fig. 7 shows the FTIR spectra collected during EEOR for the electrocatalysts as a function of the potential in 0.5 mol L^{-1} H_2SO_4 +1.0 mol L^{-1} ethanol. The information obtained from *in-situ* ATR-FTIRS provides information about the products from ethanol electro-oxidation on the catalyst surface and/or in a thin layer, as it was mentioned by other authors [16]. Bands corresponding to the C—OH stretching of acetic acid (1281 cm^{-1}) [49], O—C—O stretching of the hydrated form of acetaldehyde (931 cm^{-1}) [50,51] and O—C—O asymetric stretching of CO_2 (2342 cm^{-1}) [52] were measured. Other spectral bands can be observed at 1715, ~1200 and 1041 cm^{-1}. These bands may be ascribed to the C=O stretch of the carbonyl group of the acetic acid and acetaldehyde, the bisulfate of sulfuric acid [53] and the C—O stretching vibration in ethanol [54], respectively. Considering what they stand for, then we analyze the possibles EEOM for the different samples based on appearance or disappearance peaks in the FTIR spectra. Before this, it is appropriate to discuss the possible overlap of the acetic acid band at 1281 cm^{-1} with the band asociated to HSO_4^- at 1200 cm^{-1}. Based on the literature [22], an increase of the band intensity is expected for both species. Also, we know that other authors [20,21] have been carried out the spectroelectrochemistry experiments using $HClO_4$ as a base electrolyte instead of H_2SO_4, maybe to prevent overlap of the HSO_4^- band with the acetic acid band. However, in our work we wanted to make the spectroelectrochemistry measurements with sulfuric acid as a base electrolyte with the aim to give a new contribution to the state of the art of ethanol electro-oxidation, taking into account that there may be an effect of the anion of the base electrolyte in the ethanol electro-oxidation mechanism [23]. Even, it has already been discussed at length in the Iwasita's book chapter publication [18] that the effect of the HSO_4^- anion in the methanol reaction mechanism. We believe that H_2SO_4 base electrolyte may have a similar effect on the ethanol electro-oxidation. Thus, we think that our work will provide scientific information that will contribute to discuss the effect of the sulfuric acid media in the EEO.

Anyway, in our case, the detection of the acetate band in 1281 cm^{-1} related to the acetic acid has been possible, differing significantly from the band corresponding to HSO_4^-. Therefore, for the purposes of our work, we considered acceptable the information obtained from the *in-situ* ATR-FTIR spectra using the sulfuric acid as base electrolyte.

Continuing the discussion regarding the differents possibles EEOMs, considering that for all samples a positive directional band is observed in 1281 cm^{-1} associated with the formation of acetic acid, to a higher or lesser extent, the ethanol electro-oxidation in these electrocatalysts runs through the route that leads to the formation of acetic acid as a final product, with four electrons produced per oxidized ethanol molecule [55,56]. That has been one of the proposed and confirmed by several authors routes for ethanol oxidation in acidic electrolytes for catalysts supported on different materials [16,19,20,40,56]. Also, a peak at 931 cm^{-1} corresponding to the formation of acetaldehyde, is clearly observed for all samples. Therefore, in addition to acetic acid, ethanol oxidation lead to the formation of acetaldehyde as intermediate and/or final product, with two electrons produced per oxidized ethanol molecule [55,56]. The band instensities of acetaldehyde at 931 cm^{-1} and acetic acid at 1281 cm^{-1} as a function of the electrode potential are represented in Fig. 8. The potential at which begins to visualize the presence of acetaldehyde and acetic acid varies according to the electrocatalyst used. In the aBCs supported electrocatalysts, acetaldehyde begins to be observed in 0.2 V *vs.* Ag/AgCl electrode for PtSn/p-BC and in 0.4 V for the PtSn/c-BC, while for aVCs supported catalysts is in 0.5 V. This is consistent with the linear sweep voltammetries results where lower E_{onset} values were observed for the BCs supported catalysts. For all samples, a significant acetic acid band intensity can only be seen in a potentials higher than 0.6 V *vs* Ag/AgCl electrode although at this potential has already formed appreciable amounts of acetaldehyde. These features suggest that the conversion rate of acetaldehyde to acetic acid is very low for all electrocatalysts. Fig. 8c shows that for the PtSn/p-BC electroctalyst the acetaldehyde production from the ethanol electro-oxidation is very fast in the range of 0.3–0.4 V *vs* Ag/AgCl electrode, and then, from 0.6 V the acetic acid formation is similarly swift. These behaviors would apparently related to the shoulder observed in the linear sweep voltammograms of the PtSn/p-BC electrocatalyst.

Moreover the acetaldehyde and acetic acid peak, in the FTIR spectra, the peak around 2342 cm^{-1} (associated with the presence of CO_2) is hardly visualized only in a 1.0 V for all samples. On the one hand, this is in agreement with the inhibition of CO_2 production in the EEOR caused by the Sn in this type of alloys [20]. Although in Ref. [20] the authors can observe the formation of CO_2 in a one PtSn/C electrocatalyst sample, in the same article the authors have seen that another PtSn based electroctalyst sample show that the peak corresponding to CO_2 is much lower for all electrode potentials. This behavior was explained taking into account the affirmation of Gupta et al. [57] mentioning that when Pt is alloyed with Sn, the Pt–Pt distance is increased, and the ability of Pt to dissociate the C—H bonds of the adsorbed ethanol molecules is inhibited. Therefore, the deactivation of ethanol C—H bonds favors the production of acetic acid and not CO_2. Also, Léger et al. [40] found that the

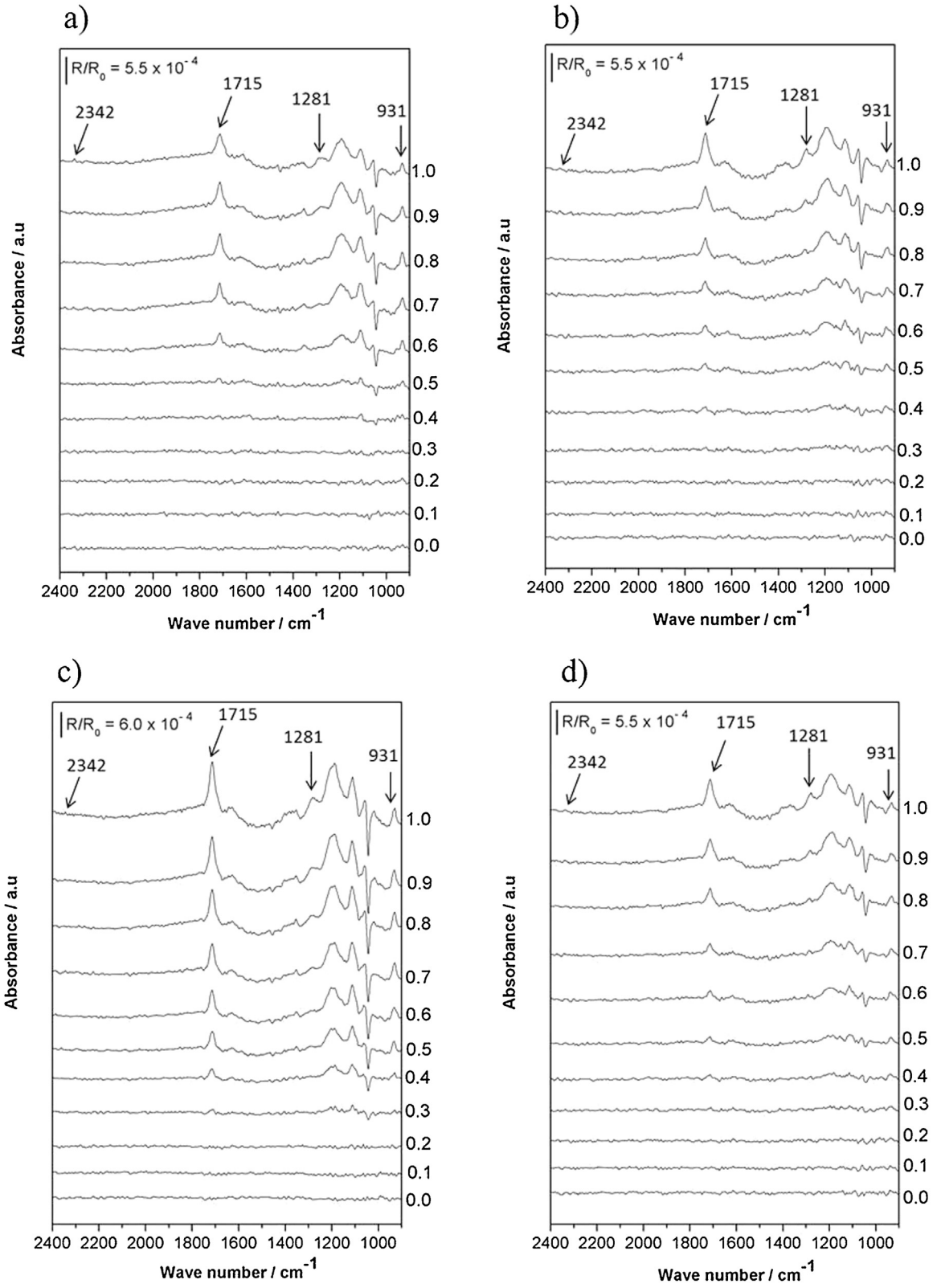

Fig. 7. ATR-FTIR *in situ* spectra taken at several potentials (indicated in volts on the right y-axis) in 0.5 mol L^{-1} H_2SO_4 +1.0 mol L^{-1} ethanol for (a) p-V and (b) c-V (c) p-BC, (d) c-BC. Backgrounds were collected at −0.15 V (Ag/AgCl).

relative intensity of the FTIR absorption band due to CO_2 at Pt-Sn/C and Pt-Sn-Ru/C electrocatalysts is lower than that obtained at Pt/C electrocatalyst, suggesting that less CO_2 is formed during the EEO on electrocatalysts with the Sn and/or Ru addition.

Additionaly to the characteristics of the PtSn nanocatalyst, the base electrolyte used in this experiments may have a fundamental role in the fact that the EEOM not occurs through in the pathway of CO and CO_2 formation. Based in previus published works,

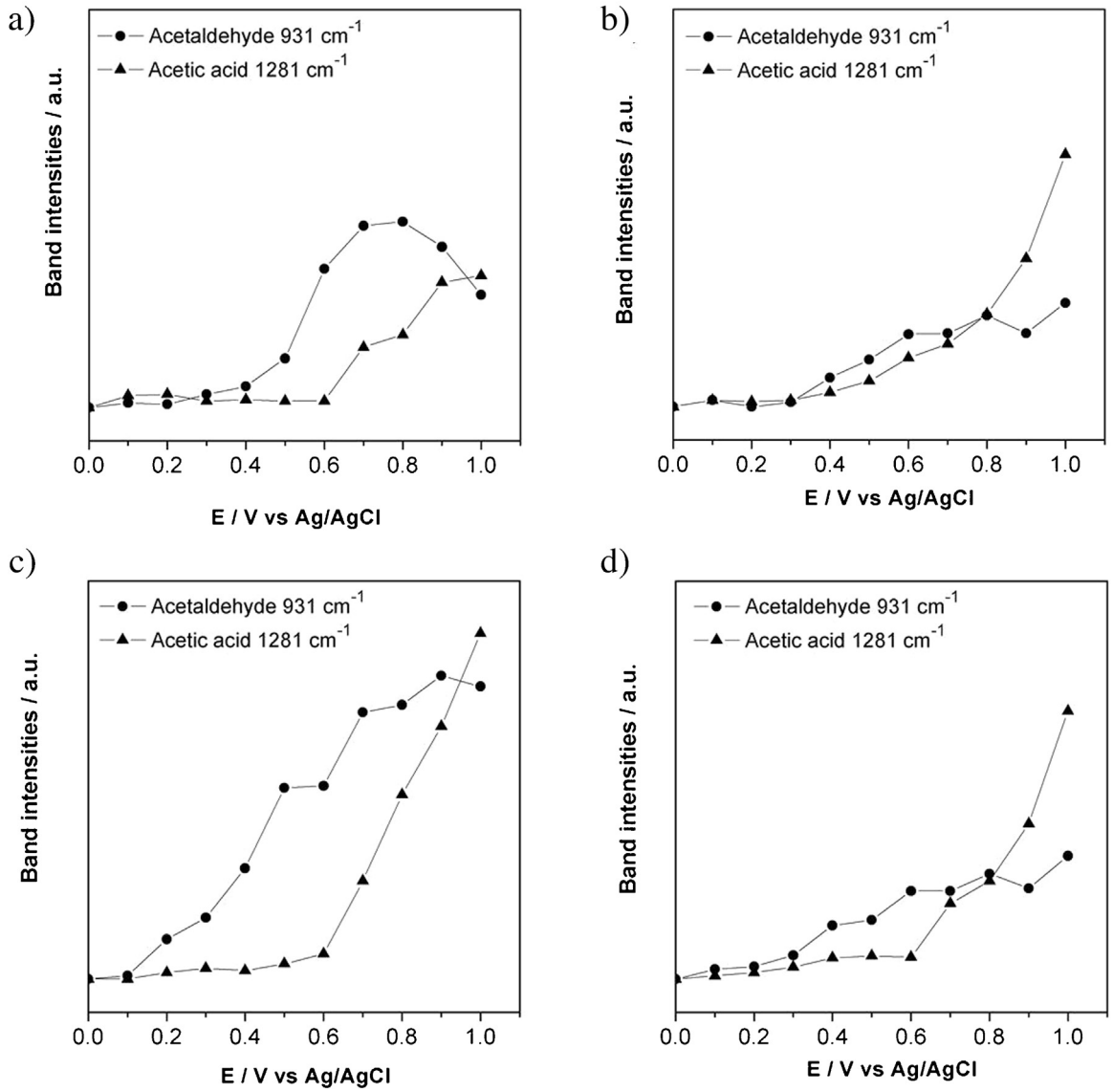

Fig. 8. Acetaldehyde and acetic acid band intensities as a function of the potential for (a) PtSn/p-V, (b) PtSn/c-V, (c) PtSn/p-BC and (d) PtSn/c-BC.

Iwasita and Camara [18] afirm that there is a differential behavior of the base electrolyte towards the different parallel pathways of methanol electro-oxidation when sulfuric acid is used as a base electrolyte. In this case, the pathway *via* CO_2 formation is inhibited due the dissociative adsorption of methanol is strongly hindered by adsorbed bisulfate, and in consequence, adsorbed CO and CO_2 are not produced and therefore they are not detected in the *in-situ* FTIRS experiments. These phenomena may also be occurring in the case of the ethanol electro-oxidation using sulfuric acid as a base electrolyte. This would explain why it was CO and CO_2 are not significantly detected in our spectroelectrochemical analysis.

It summary, from the *in-situ* ATR-FTIRS experiments, it can be concluded for all the studied supports, that the preferred route for EEOR in sulfuric acid media leads to the formation of acetic acid with acetaldehyde production.

Regarding the aforementioned discussions, the catalyst support have influence on the morphology and deposition of the catalyts that can enhance their catalytic activity. However, the nature of the support and the activation method do not modify the electro-oxidation in sulfuric acid.

4. Conclusion

The impregnation/reduction method using ethylene glycol as a reducing agent is a suitable method for obtaining carbon supported PtSn nanoparticles. The nature of the support and the activation method have influence in the morphological and structural characteristics of the PtSn based electrocatalysts. On the aBCs, PtSn particles are agglomerated and distributed throughout the whole support, when compared to the ones on the Vulcan-based carbons, where the catalyst deposition was agglomerate and concentered on some regions of the support. The electrocatalytic performance of aBCs supported catalysts is better than that of the activated Vulcan carbons supported ones, since they show higher electrochemically active surface area, lower onset potential and greater current density for the EEO in sulfuric acid media. The better electrochemical performances for the aBCs corresponded to the obtained by physical activation. By *in-situ* ATR-FTIRS, it was determined that the EEO on the studied PtSn electrocatalysts, using sulfuric acid as base electrolyte, occurs mainly through the acetic acid and acetaldehyde production, regardless of the support.

Acknowledgements

The present work was carried out with support of CAPES (project CAPES /UdelaR N° 044/2011), Brazilian Government entity focused in human resources formation. The authors would also like to thank the CNPq. A. Cuña thanks the Brazilian CAPES for the grant received (Bolsista CAPES/Brasil).

References

[1] J. Asgardi, J.C. Calderón, F. Alcaide, A. Querejeta, L. Calvillo, M.J. Lázaro, G. García, E. Pastor, Appl. Catal. B 168 (2015) 33–41.
[2] L. Calvillo, V. Celorrio, R. Moliner, A.B. Garcia, I. Camean, M.J. Lazaro, Electrochim. Acta 102 (2013) 19–27.
[3] N. Nakagawa, Y. Ito, T. Tsujiguchi, H. Ishitobi, J. Power Sources 248 (2014) 330–336.
[4] L.M. Ombaka, P. Ndungu, V.O. Nyamori, Catal. Today 217 (2013) 65–75.
[5] L. Yuan, L. Jiang, J. Liu, Z. Xia, S. Wang, G. Sun, Electrochim. Acta 135 (2014) 168–174.
[6] E.L. Silva, M.R. Ortega Vega, P.S. Correa, A. Cuña, N. Tancredi, C.F. Malfatti, Int. J. Hydrogen Energy 39 (2014) 14760–14767.
[7] E. Antolini, Appl. Catal. B 88 (2009) 1–24.
[8] A. Amaya, N. Medero, N. Tancredi, H. Silva, F. Sardella, C. Deiana, Bioresour. Technol. 98 (2007) 1635–1641.
[9] A. Amaya, J. Píriz, N. Tancredi, T. Cordero, J. Therm. Anal. Calorim. 89 (2007) 987–991.
[10] N. Tancredi, T. Cordero, J. Rodríguez Mirasol, J. Rodríguez, Fuel 75 (75) (1996) 1701–1706.
[11] A. Cuña, N. Tancredi, J. Bussi, V. Barranco, T.A. Centeno, A. Quevedo, J.M. Rojo, J. Electrochem. Soc. 161 (2014) A1806–A1811.
[12] A. Cuña, N. Tancredi, J. Bussi, C. Deiana, M.F. Sardella, V. Barranco, J.M. Rojo, Waste Biomass Valorization 5 (2014) 305–313.
[13] J. Asgardi, J.C. Calderón, F. Alcaide, A. Querejeta, L. Calvillo, M.J. Lázaro, G. García, E. Pastor, Appl. Catal. B 168–169 (2015) 33–41.
[14] L. Calvillo, V. Celorrio, R. Moliner, M.J. Lázaro, Mater. Chem. Phys. 127 (2011) 335–341.
[15] M. Carmo, A.R. dos Santos, J.G.R. Poco, M. Linardi, J. Power Sources 173 (2007) 860–866.
[16] R.F.B. De Souza, J.C.M. Silva, F.C. Simoes, M.L. Calegaro, A.O. Neto, M.C. Santos, Int. J. Electrochem. Sci. 7 (2012) 5356–5366.
[17] T. Iwasita, F.C. Nart, Prog. Surf. Sci. 55 (1997) 271–340.
[18] T. Iwasita, G.A. Camara, in: S.-G. Sun, P.A. Christensen, A. Wieckowski (Eds.), In-situ Spectroscopic Studies of Adsorption at the Electrode and Electrocatalysis, Elsevier B.V., Amsterdam, 2007, pp. 33–61.
[19] M.H.M.T. Assumpção, J. Nandenha, G.S. Buzzo, J.C.M. Silva, E.V. Spinacé, A.O. Neto, R.F.B. De Souza, J. Power Sources 253 (2014) 392–396.
[20] J.C.M. Silva, L.S. Parreira, R.F.B. De Souza, M.L. Calegaro, E.V. Spinacé, A. Oliveira Neto, M.C. Santos, Appl. Catal. B 110 (2011) 141–147.
[21] R.F.B. De Souza, L.S. Parreira, J.C.M. Silva, F.C. Simoes, M.L. Calegaro, M.J. Giz, A.O. Neto, M.C. Santos, Int. J. Hydrogen Energy 36 (2011) 11519–11527.
[22] M. Heinen, Z. Jusys, R.J. Behm, J. Phys. Chem. 114 (2010) 9850–9864.
[23] M.E. Paulino, L.M.S. Nunes, E.R. Gonzalez, G. Tremiliosi-Filho, Electrochem. Comm. 52 (2015) 85–88.
[24] T.E. Rufford, D. Hulicova-Jurcakova, Z. Zhu, G.Q. Lu, J. Power Sources 195 (2010) 912–918.
[25] P.S. Correa, E.L. Silva, R.F. da Silva, C. Radtke, B. Moreno, E. Chinarro, C.F. Malfatti, Int. J. Hydrogen Energy 37 (2012) 9314–9323.
[26] Lowell, J.E. Shields, Powder Surface Area and Porosity, Chapman and Hall Ltd, London, 1984, pp. 61–62.
[27] F. Stoeckli, T.A. Centeno, J. Mater. Chem. A 1 (2013) 6865–6873.
[28] D28 Committee, Test method for total ash content of activated carbon, ASTM Int., 2011.
[29] M. Carmo, A.R. dos Santos, J.G.R. Poco, M. Linardi, J. Power Sources 173 (2007) 860–866.
[30] M. Watanabe, H. Sei, P. Stonehart, J. Electroanal. Chem. 261 (1989) 375.
[31] H. Marsh, R.F. Rodríguez-Reinoso, Activated Carbons, Elsevier, Oxford, UK, 2006.
[32] Misra, et al., Biomass Bioenergy 4 (1993) 103–116.
[33] M.J. Lambert, Inorganic constituents in wood and bark of new south wales forest tree species forestry, in: Forestry Commission of New South Wales, Australian National Library, Sidney, 1981.
[34] W. Zhou, Z. Zhou, S. Song, W. Li, G. Sun, P. Tsiakaras, et al., Appl. Catal. B 46 (2003) 273–285.
[35] M. Chatterjee, A. Chatterjee, S. Ghosh, I. Basumallick, Electrochim. Acta 54 (2009) 7299–7304.
[36] F. Colmati, E. Antolini, E.R. Gonzalez, Appl. Catal. B 73 (2007) 106–115.
[37] J.H. Kim, S.M. Choi, S.H. Nam, M.H. Seo, S.H. Choi, W.B. Kim, Appl. Catal. B 82 (2008) 89–102.
[38] W.S. Cardoso, M.S.P. Francisco, A.M.S. Lucho, Y. Gushiken, Solid State Ionics 167 (2004) 165.
[39] E.V. Spinacé, M. Linardi, A.O. Neto, Electrochem. Commun. 7 (2005) 365–369.
[40] J.-M. Léger, S. Rousseau, C. Coutanceau, F. Hahn, C. Lamy, Electrochim. Acta 50 (2005) 5118–5125.
[41] P. Serp, B. Machado, Nanostructured Carbon Materials for Catalysis, Royal Social of Chemistry, London, 2015.
[42] P.A. Marsh, A. Voet, T.J. Mullens, L.D. Price, Carbon 9 (1971) 797–805.
[43] M.C. Roman-Martinez, D. Cazorla-Amoros, A. Linares-Solano, C.S.-M. De Lecea, H. Yamashita, M. Anpo, Influence of the support surface chemistry, Carbon 33 (1995) 3–13.
[44] F. Rodríguez-Reinoso, Carbon 36 (1998) 159–175.
[45] H.F. Stoeckli, Carbon 28 (1990) 1–6.
[46] M. Inagaki, F. Kang, M. Toyoda, H. Konno, Advanced Materials Science and Engineering of Carbon, Elsevier, New York, 2014.
[47] B.E. Conway, Electrochemical supercapacitors, in: Scientific Fundamentals and Technological Applications, Kluwer Academic/Plenum Publishers, New York, 1999.
[48] L. Zheng, L. Xiong, Q. Liu, K. Han, W. Liu, Y. Li, K. Tao, L. Niu, S. Yang, J. Xia, Electrochim. Acta 56 (2011) 9860–9867.
[49] G. Socrates, Infrared Characteristic Group Frequencies, Wiley, New York, 1996.
[50] S.C. Chang, L.-M. Leung, M.J. Weaver, J. Phys. Chem. 94 (1990) 6013–6021.
[51] L.-W. Leung, S.C. Chang, M.J. Weaver, J. Electroanal. Chem. 266 (1989) 317–336.
[52] J.C. Morris, J. Chem. Phys. 11 (1943) 230–235.
[53] P.W. Faguy, N. Markovic, R.R. Adzic, C.A. Fierro, E.B. Yeager, J. Electroanal. Chem. 289 (1990) 245–262.
[54] E.K. Plyler, J. Res. Natl. Bur. Stand. 48 (1952) 281–286.
[55] F. Colmati, G. Tremiliosi-Filho, E.R. Gonzalez, A. Berná, E. Herrero, J.M. Feliu, Faraday Discuss. 140 (2008) 379–397.
[56] M.C. Figueiredo, A. Santasalo-Aarnio, F.J. Vidal-Iglesias, J. Solla-Gullón, J.M. Feliu, K. Kontturi, T. Kallio, Appl. Catal. B 140 (2013) 378–385.
[57] S. Sen Gupta, S. Slingh, J. Datta, Mater. Chem. Phys. 120 (2010) 682–690.